CrossMark

# Evaluation of VOC fluxes at the soil-air interface using different flux chambers and a quasi-analytical approach

**Solenn Cotel · Gerhard Schäfer · Sylvie Traverse ·
Salsabil Marzougui-Jaafar · Guillaume Gay ·
Olivier Razakarisoa**

**Abstract** Dense nonaqueous-phase liquids (DNAPLs) spilled on the soil migrate vertically depending upon gravity and capillary forces through the unsaturated zone of the porous aquifer, forming a vapour plume. These volatile organic compounds (VOCs) can be transferred by advection-diffusion to the groundwater or to the atmosphere. Evaluating DNAPL vapour fluxes at the soil-air interface is one of the key challenges in the remediation of contaminated sites. This work discusses the results of a large-scale vapour plume experiment with a well-defined trichloroethylene (TCE) spill, including a sequential raising and lowering of the water table, where the TCE vapour fluxes at the soil surface were experimentally quantified in two ways: (i) directly, with measurements at the soil-air interface using different flux chambers at various operational modes under both transient and steady-state conditions of the vapour plume, and (ii) indirectly, using a quasi-analytical approach based on soil gas measurements. It was shown that upward displacement of the water-air front during the controlled raising of the water table (approximately $10 \text{ cm h}^{-1}$) increased the TCE vapour flux measured at the soil surface by factors of 4 to 10. Under steady-state transport conditions, TCE vapour fluxes measured using five types of flux chambers and three operational modes were similar. The effects of the flux chamber geometry, the accumulation of TCE vapours in the chamber headspace or the air recirculation at a low flow rate on the measured TCE vapour fluxes were low. At steady-state transport conditions, TCE vapour fluxes measured with the flux chambers and estimated using the quasi-analytical approach were of the same order of magnitude. However, under transient conditions of the vapour plume, the TCE vapour flux predicted by the quasi-analytical approach greatly underestimated or overestimated the real TCE vapour flux at the soil-air interface.

S. Cotel · G. Schäfer (✉) · S. Marzougui-Jaafar ·
O. Razakarisoa
Laboratoire d'Hydrologie et de Géochimie de Strasbourg (LHyGeS), UMR 7517, Université de Strasbourg - Centre National de la Recherche Scientifique (CNRS), 1 rue Blessig, 67084 Strasbourg, France
e-mail: schafer@unistra.fr

S. Traverse
BURGEAP, 19 Rue de la Villette, 69003 Lyon, France

G. Gay
INERIS, Parc Technologique ALATA, 60550 Verneuil-en-Halatte, France

*Present Address:*
G. Gay
present adress: Direction Régionale et Interdépartementale de l'Environnement et de l'Energie (DRIEE), 10 rue Crillon, 75194 Paris, France

## 1 Introduction

In many countries, industrialisation and technological development have led to increased use of dense nonaqueous-phase liquids (DNAPLs) such as

chlorinated solvents, e.g., trichloroethylene (TCE). Where these volatile organic compounds (VOCs) were accidentally spilled on the soil during transport or leaked from their storage places, large DNAPL vapour plumes and long-term solute plumes in the groundwater developed. Many recent studies have shown the high toxicity of TCE (Bahr et al. 2011; Rusyn et al. 2014). Solute plumes may have a serious direct impact on the quality of groundwater and soils. Vapour plumes often affect the quality of outdoor air by VOC fluxes from the vadose zone to the atmosphere and the quality of air inside buildings by migration of VOCs from the vadose zone through concrete floor slabs. Transport of VOCs in the vadose zone is primarily due to diffusion (Pankow and Cherry 1996; Choi et al. 2002; Jellali et al. 2003; Bohy et al. 2006). However, advection can also contribute to mass transport of VOCs. Advective mass fluxes can be generated by density gradients within and along the fringe of the vapour plume (Sleep and Sykes 1989; Lenhard et al. 1995; Pankow and Cherry 1996; Cotel 2008; Cotel et al. 2011) or by pressure gradients caused, for example, by variations in atmospheric pressure (Massmann and Farrier 1992; Pasteris et al. 2002) or by volatilisation of the DNAPL (Baehr and Bruell 1990; Altevogt et al. 2003).

The impact of soil or groundwater contamination on indoor or outdoor air is directly linked to the VOC vapour flux from the subsurface to the building or atmosphere. From a technical point of view, it is important to quantify this flux of pollutant (Baker et al. 2011; Traverse et al. 2013) because it may help to locate and identify source zones in the subsurface, to interpret VOC concentrations measured in indoor or outdoor air, to plan remediation processes or to contribute to the modelling of mass transfer in the atmosphere and vadose zone. Since the 1970s, a variety of direct or indirect experimental approaches have been used for the assessment of volatile pollutant flux to the atmosphere. Vapour fluxes can be directly measured at the soil-air interface using static flux chambers (recent examples include Wang et al. 2013; Pihlatie et al. 2013; Parker et al. 2013a; Sihota et al. 2013; Collier et al. 2014; Gallego et al. 2014; Happell et al. 2014; Miola et al. 2015) or using open or closed dynamic flux chambers (recent examples include Ma et al. 2013; Parker et al. 2013a; Parker et al. 2013b; Sihota et al. 2013; Carpi et al. 2014; Liu et al. 2014; Miola et al. 2015). By definition, dynamic flux chambers differ from static flux chambers by the presence of a more or less

high forced air flow passing through the measuring device (Hudson and Ayoko 2008). Vapour fluxes can also be indirectly quantified using either a quasi-analytical approach based on Fick's first law and soil gas measurements (recent examples include Marzougui et al. 2012; Happell et al. 2014; Maier and Schack-Kirchner 2014) or micrometeorological methods based on atmospheric measurements (recent examples include Wang et al. 2013; Yu et al. 2013). As flux chambers are universally applicable, easy to set up, usually low cost and allow for direct flux measurement, they have been widely used for assessing emissions of mercury, pesticides, fertilisers, and greenhouse gases to the atmosphere. However, they have been used little for assessing emissions of nonmethane VOCs from a subsurface source (Eklund et al. 1985; Batterman et al. 1992; Smith et al. 1996; Jellali et al. 2003).

Because all chamber types affect the object being measured, each chamber type has its own limitations (Davidson et al. 2002; Pumpanen et al. 2004). The main disadvantages of dynamic flux chambers are the strong dependence on the measured flux of the applied flushing air flow (Gao and Yates 1998; Wallschläger et al. Wallschlager et al. 1999; Lindberg et al. 2002; Eckley et al. 2010; Gallego et al. 2014) and of any significant air pressure difference between the inside and outside of the chambers (Kanemasu et al. 1974; Lund et al. 1999; Davidson et al. 2002; Pumpanen et al. 2004). The often-cited disadvantages of static flux chambers are underestimation of the pollutant vapour flux due to a pressure increase in the chamber headspace during installation of the device (Pumpanen et al. 2004; Christiansen et al. 2011; Rochette 2011; Gallego et al. 2014) or due to pollutant accumulation in the chamber headspace after starting the measurements (Gao and Yates 1998; Davidson et al. 2002; Pumpanen et al. 2004; Hudson and Ayoko 2008) or disturbances of the pollutant vapour flux due to punctuated gas sampling (Bekku et al. 1995; Christiansen et al. 2011). At a low flushing air flow, dynamic chambers produce the same underestimation of the pollutant vapour flux as static flux chambers due to pollutant accumulation in the chamber headspace after starting the measurement (Gao and Yates 1998; Lindberg et al. 2002; Eckley et al. 2010). A pollutant vapour accumulation in the chamber headspace decreases the vapour gradient between the near-surface soil air and the chamber indoor air and thus decreases the natural diffusive flux crossing the soil surface. Positive and negative relative driving

pressures between the chamber indoor air and the near-surface soil air generate artificial advective vapour fluxes across the soil surface, and thus modify the vapour flux measured in the flux chamber. Moreover, except the flux chamber designed by Tillman (2003), all static flux chambers, which are closed by definition, and closed dynamic chambers allow for quantification of only the diffusive part of the total vapour flux emitted by the underlying subsurface source zone.

In the past, a large number of flux chambers differing greatly in shape, size and operating conditions have been used to measure vapour fluxes (Hudson and Ayoko 2008). Studies comparing the measured flux using various devices indicated substantial differences (Lindberg et al. 2002; Pumpanen et al. 2004; Eckley et al. 2010; Pihlatie et al. 2013). Regardless of any air pressure difference between the inside and outside of the chamber, these differences have been explained by the operation mode (static or dynamic) or the choice of the flow rate of air flushing in dynamic flux chambers, by the geometric characteristics of the flux chamber (Pihlatie et al. 2013; Eckley et al. 2010) or by the lack or an excessive speed of a mixing fan in the chamber headspace (Christiansen et al. 2011; Pumpanen et al. 2004).

The paper reports new findings on methodological aspects of and uncertainties in the evaluation of DNAPL vapour fluxes at the soil surface under both transient and steady-state conditions of the vapour plume. The pollutant chosen was TCE, the solvent that is found most frequently in groundwater throughout the world (Lerner et al. 1991). We discuss the results of large-scale vapour plume experiments with a well-defined TCE spill, including a sequential raising and lowering of the water table, in which the TCE vapour fluxes at the soil surface were experimentally quantified in two ways: (i) directly, with measurements at the soil-air interface using various closed flux chambers and operational modes under both transient and steady-state conditions of the vapour plume, and (ii) indirectly, using a quasi-analytical approach based on soil gas and water content measurements and taking into account Fickian diffusion and advection. The tested operational modes of the flux chambers included a static configuration and two closed dynamic configurations at very low flow rates of air flushing. In one of the two dynamic configurations, a carbon trap was used to limit the accumulation of TCE vapour in the chamber headspace. A few studies used flux chambers that limit pollutant vapour accumulation

in the headspace (Nômmik 1973; Nay et al. 1994; Tillman et al., 2003; Miola et al. 2015), but the nonsorbed pollutant part could not be taken into account. In our method of limiting the TCE vapour accumulation in the chamber headspace, the sorbed and nonsorbed pollutant parts were taken into account in vapour flux calculations. The use of this quasi-analytical approach in parallel with the direct measurement of the vapour flux using flux chambers allowed not only a comparison of estimated TCE vapour fluxes with those measured but also the assessment of the advective part of the TCE vapour flux that is not taken into account by traditional closed flux chamber measurements. The tests of the various operational modes of the flux chambers focused on the effect of both the accumulation of the TCE vapour in the chamber headspace and the air circulation on the estimation of the diffusive mass flux. The tests of the various flux measurement devices using the same operational mode allowed for highlighting of the impact of the geometry of the flux chamber on the measured TCE flux.

## 2 Materials and methods

### 2.1 Experimental setup

The Site Contrôl Exp rimental de Recherche pour la r habilitation des Eaux et des Sols (SCERES) facility is a watertight basin that is 25 m long, 12 m wide and 3 m deep which is protected against rainfall by a fixed roof (Fig. 1). The hydraulic gradient, flow rate, water table levels and water sampling can be managed and monitored in two pits located at the upstream and downstream ends of the basin. SCERES recreates a three-layer alluvial aquifer system with two local less-permeable inclusions. The three-layer aquifer from top to bottom was composed of fine-grained sand with a thickness of 0.5 m (hydraulic conductivity $K{\sim}0.00005$ m s$^{-1}$), a medium-grained sand with a low organic content (foc=0.09 %, based on NF T 31-109) and a thickness of 2 m (hydraulic conductivity $K{\sim}0.0008$ m s$^{-1}$), and coarser sand with a thickness of 0.5 m ($K{\sim}0.006$ m s$^{-1}$). The two local less-permeable inclusions composed of the fine-grained sand measured 1 m×1 m×0.5 m and 2 m×2 m×0.8 m and were inserted in the medium-grained sand 7.5 to 8.5 m from the upstream wall and 5.5 to 6.5 m from the lateral wall and 7.5 to 9.5 m from the upstream wall and 5 to 7 m

from the lateral wall, respectively (Fig. 1). An artificially fissured concrete slab with a thickness of 0.13 m ($K\sim0.00002$ m s$^{-1}$) was placed on the surface of the SCERES model over a 0.13-m-thick gravel layer.

The experimental setup has been the subject of various large-scale studies (recent examples include Dridi et al. 2009; Marzougui-Jaafar 2013; Traverse et al. 2013). The basin was equipped with many measuring devices (e.g., anemometers, thermo-hydrometers, time-domain reflectometers, capacitive probes, and pressure probes), several monitoring wells and a spatial network of air and water sampling points at various depths (Fig. 1). Gas sampling was performed using 1-cm-internal-diameter copper tubes fitted at their tips with a 4-cm-long screened head and covered with textile membranes. Available sampling depths were 0.2, 0.4, 0.6 and 0.9 m. The piezometer used in this study, designated P4, was located near the TCE source zone. The relative pressure measurements of the soil air were performed using high-sensitivity pressure probes (Greisinger GMH 3151) connected to flexible Teflon tubes fitted at their tip with a hydrophobic cup driven into the soil. Relative pressure measurements were taken at depths of 0.25, 0.45, 0.65 and 1.25 m. The vertical water content profile of the porous medium was measured using capacitive probes (Sentek EnviroSMART). Water content profile S2 crossed the fine and medium sand layers, whereas profile S1 also crossed the two low-permeability block inclusions. The depth of investigation was 1.45 m along S1 and 1.95 m along S2, with near-surface measurements at 0.15 and 0.25 m along S1 and at 0.05, 0.15 and 0.25 m along S2.

### 2.2 Experimental conditions

DNAPL vapour migration experiments were conducted in the unsaturated zone of the artificial alluvial aquifer
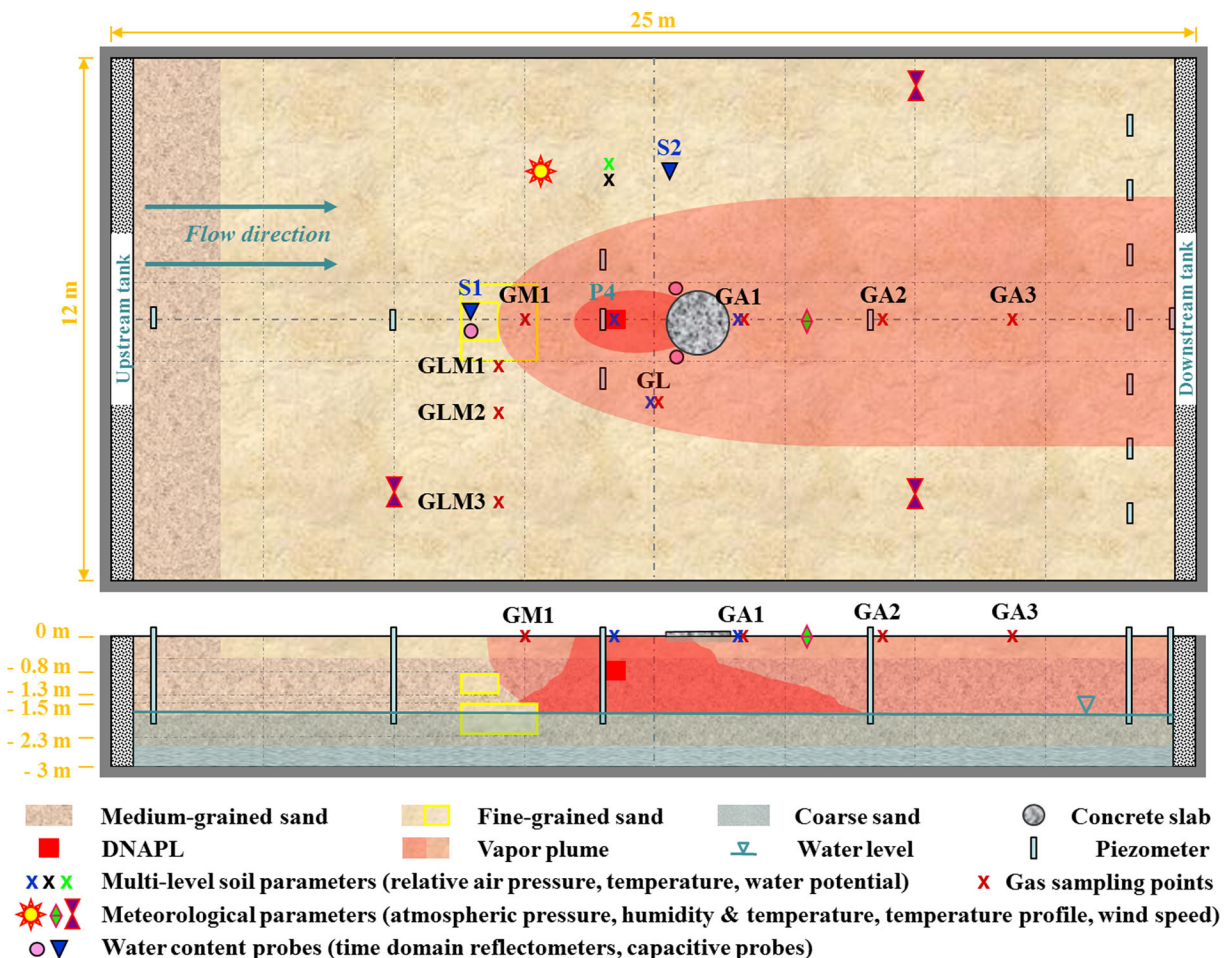


Fig. 1 Top view and central vertical cross section of the SCERES facility (Strasbourg-Cronenbourg, France)

for 2 months in 2011 and 2012 (Marzougui-Jaafar 2013). To create a DNAPL source zone, 3.9 and 5.5 L of TCE as a pure phase were allowed to infiltrate the vadose zone in 2011 and 2012, respectively, 0.55 m beneath the soil surface, between 10.85 m and 11.35 m from the upstream wall and 5.75 m from both lateral walls. Day 0 of each experiment was the day of the creation of the source zone. The injection device was described in detail by Marzougui-Jaafar (2013). The main hydraulic conditions of this study were defined by a 1.2-m-thick saturated zone, a pore water velocity of 0.85 m day$^{-1}$ in the medium sand and a highly water-saturated level at the base of the fine sand (see Fig. 1). In the 2011 experiment, 50 cm of raising followed up by 50 cm of lowering of the water table were created, respectively, on days 31 and 33. Raising and lowering of the water table in the SCERES facility were realised by raising and lowering weirs located in technical pits and connected to the upstream and downstream tanks. In the platform centre, the maximum rates of raising and lowering of the water table were approximately 1.7 and 2.1 cm in 10 min, respectively. Later, the spatial distribution of the TCE vapour plume was strongly modified during various experiments conducted at the soil/air interface or on the concrete slab. For example, on day 26, mass flux tests across the concrete slab were performed. Eight days later, the existing slab was replaced by a more-permeable concrete slab to change the boundaries conditions of the vapour plume within the frame of another experiment (Marzougui-Jaafar 2013). Then, on day 38, other mass flux tests across the concrete slab were conducted, and between day 43 and day 47, additional flux chamber tests were performed.

TCE vapour fluxes were measured at sampling points GM1, GA1 and GL, which were located, respectively, upstream, downstream and laterally of the TCE source zone (see Fig. 1). The distances between GM1, GA1 and GL and the source zone centre were 2.1, 2.95 and 2.1 m, respectively. Vertical TCE vapour fluxes were experimentally determined in two ways: by direct flux monitoring at the soil-air interface using flux chambers (see Sect. 2.3) and by flux evaluation based on near-soil surface measurements of TCE concentrations in the soil air using a quasi-analytical approach (see Sect. 2.4).

## 2.3 Vapour flux monitoring at the soil surface using flux chambers

To monitor the TCE vapour fluxes at the soil surface, five flux chambers, designated CF1, CF2, CF3, CF4 and CF5

(Table 1), were used. The majority of the measuring devices were installed on the surface of the facility by embedding the chamber edges 3 cm deep in the soil, except for CF1, which was placed on the soil surface. Only CF2 and CF4 were equipped with a small fan to homogenise the TCE vapour concentration in the chamber headspace. The individual cross sections and volumes ranged, respectively, from 7 to 25 dm$^2$ and from 3 to 64 L.
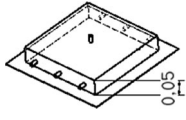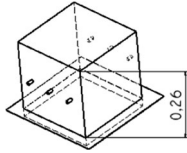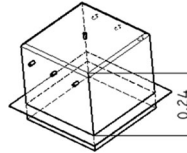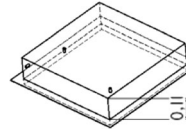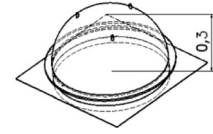
Flux measurements were performed in three ways: (i) with TCE vapour accumulation in the chamber and occasional concentration measurements in the chamber (method used by Pihlatie et al. 2013; Sihota et al. 2013; Wang et al. 2013; Yu et al. 2013; Happell et al. 2014), (ii) with TCE vapour accumulation in the chamber and applying a recirculation of air at a low flow rate (method used by Di Francesco et al. 1998; Pumpanen et al. 2004; Christiansen et al. 2011), and (iii) without TCE vapour accumulation in the chamber and applying air recirculation at a low flow rate (method used by Jellali et al. 2003). The absence of vapour accumulation in the chamber was due to a carbon trap (Supelco, activated carbon trap Orbo 32) placed in the air recirculation circuit. With method (i), the total sampled volume for pollutant concentration measurements was low compared to the internal volume of the flux chambers. With methods (ii) and (iii), the flux chambers worked in a closed-circuit manner with recirculation of the vapours to avoid forced suction of soil gas. The flux chambers using method (i) were so-called static flux chambers, whereas flux chambers using methods (ii) and (iii) were so-called closed dynamic flux chambers (Hudson and Ayoko 2008). Note that all three flux measurement methods allowed quantification of only the diffusive part of the TCE vapour flux crossing the soil surface because the walls of the chamber were no-flow boundaries.

TCE vapour fluxes at the soil surface ($F_{soil/atm}$ in mg m$^{-2}$ s$^{-1}$) were calculated specifically for each method. For methods (i) and (ii), TCE vapour fluxes per unit surface were quantified during the transient state of vapour transfer in the flux chamber headspace as follows (Matthias et al. 1980):

$$F_{soil/atm} = \frac{dC_{ch}}{dt} \times \frac{V_{ch}}{A_{ch}} \qquad (1)$$

where $dC_{ch}$ (mg m$^{-3}$) is the variation of the TCE vapour concentration in the chamber during $dt$ (s), $V_{ch}$ (m$^3$) is the net volume of the chamber, and $A_{ch}$ (m$^2$) is the

**Table 1** Characteristics of the flux chambers

| Name | CF1 | CF2 | CF3 | CF4 | CF5 |
|---|---|---|---|---|---|
| Pattern Height (m) |  0.05 |  0.26 |  0.24 |  0.1 |  0.3 |
| Net area (m²) | 0.066 | 0.073 | 0.088 | 0.25 | 0.20 |
| Net volume (m³) | 0.0032 | 0.019 | 0.021 | 0.028 | 0.064 |
| Material | Stainless steel | Polyvinyl chloride | High-density polyethylene | Polycarbonate | Polymethyl methacrylate |

measured area on the soil surface. Based on the principle of vapour accumulation within the chamber, the slope of the measured vapour concentration-time curve early in the test is generally used to quantify the time derivative of Eq. (1).

For method (iii), the TCE vapour flux per unit surface during a given time period was calculated using (Jellali et al. 2003) the equation

$$F_{soil/atm} = \frac{(m_{ads} + C_{ch} \times V_{ch})}{\Delta t \times A_{ch}} \quad (2)$$

where $m_{ads}$ (mg) is the TCE mass adsorbed on the charcoal trap, $C_{ch}$ (mg m$^{-3}$) is the TCE vapour concentration in the chamber headspace, and $\Delta t$ (s) is the measured time interval.

For methods (i), (ii) and (iii), the TCE vapour concentration in the chambers were measured either with portable photo-ionisation detectors (MiniRAE 2000, RAE Systems) or with a multigas monitor equipped with a photo-acoustic infrared detector (model 1312, INNOVA). The detection limit of the portable photo-ionisation detectors RAE was 0.5 mg m$^{-3}$ (at 20 °C), with an experimental relative measurement uncertainty of about 5 %. The detection limit of the multigas monitor equipped with a photo-acoustic infrared detector INNOVA was 0.4 mg m$^{-3}$ (at 20 °C), with a drift of about 2.5 % of measured value per 3 months. Additionally, for method (iii), the TCE mass adsorbed on the charcoal was analysed after desorption in hexane containing dodecane as the internal standard (Jellali et al. 2003) using gas chromatography with a flame ionisation detector (Chrompack, CP 9000). The analysis lasted 10 min, and a volume of 0.5 μL was injected in the device using on-column injection mode. The temperature of the injector was 250 °C, and the oven temperature varied between 40 and 250 °C. For method (ii), the air recirculation was produced either with the internal pump of the photo-acoustic device INNOVA or with the internal pump of a portable photo-ionisation detector, whereas for method (iii), a peristaltic pump (Masterflex) was used.

All flux measurements spanned 35 min, and for methods (ii) and (iii), the air recirculation flow rate was 0.5 L min$^{-1}$. During all measurements, the driving pressure difference between the air inside and outside of the chamber was monitored. A significant pressure difference can be generated, for example, by a high air flow rate used for air recirculation. Note that even low pressure differences of approximately 1 Pa may cause mass flux errors (Kanemasu et al. 1974; Lund et al. 1999; Pumpanen et al. 2004).

2.4 Prediction of vertical vapour fluxes based on a quasi-analytical approach

In the vadose zone, the TCE vapour flux combines a diffusive portion governed by Fick's law and an advective portion governed by the Darcy's law that depends mostly on the driving pressure gradient between the soil and the atmosphere and on the density gradient between the gas mixture (soil air containing TCE vapour) and pure soil air. Generally, the dispersive mass flux of vapours is neglected. The total TCE vapour flux in the vertical ($z$) direction $F_z$ (mg m$^{-2}$ s$^{-1}$) can be expressed as follows (Mendoza and Frind 1990; Marzougui et al. 2012):

$$F_z = -D_a^{eff} \frac{dC_a}{dz}$$
$$+ C_a \left( -\frac{k_{ra} k^* \rho_{air} g}{\mu_a} \left[ \frac{dH_a^*}{dz} + \frac{\rho_a - \rho_{air}}{\rho_{air}} \right] \right) \quad (3)$$

where $D_a^{eff}$ (m$^2$ s$^{-1}$) is the effective air diffusion coefficient, $z$ (m) is the elevation (note that in our case, z=0 corresponds to the soil surface), $C_a$ (mg m$^{-3}$) is the pollutant vapour concentration, $k_{ra}$ (−) is the relative gas permeability, $k^*$ (m$^2$) is the intrinsic permeability, $\rho_{air}$ (kg m$^{-3}$) is the density of the uncontaminated soil air, $g$ (m s$^{-2}$) is the gravity acceleration constant, $\mu_a$ (Pa s) is the dynamic gas viscosity, $H_a^*$ (m) is the pneumatic head of the gas mixture, and $\rho_a$ (kg m$^{-3}$) is the density of the gas mixture. It is assumed that the gas density is not significantly influenced by the gas pressure because the variations of pressure in time and space are not expected to be large.

The estimation of soil gas diffusivity is a major source of uncertainty in this type of quasi-analytical approach in field experiments (Maier and Schack-Kirchner 2014). In this study, to estimate the effective gas diffusion coefficient, the empirical expression developed by Millington and Quirk (1961) was used:

$$D_a^{eff} = S_a \varepsilon \tau_a D_a^0 = S_a^{10/3} \varepsilon^{4/3} D_a^0 \quad (4)$$

where $S_a$ (−) is the gas saturation of the porous medium, $\varepsilon$ (−) is the porosity, $\tau_a$ (−) is the tortuosity of the porous medium with regard to soil air and $D_a^0$ (m$^2$ s$^{-1}$) is the free air diffusion coefficient.

The diffusion coefficient, which is dependent on the temperature, was expressed by Grathwohl (1998) as follows:

$$D_a^0 = \frac{10^{-6}(T_a + 273.15)^{1.75}\sqrt{(1/M_{air} + 1/M_{TCE})}}{P_a\left(V_{air}^{1/3} + V_{TCE}^{1/3}\right)^2} \quad (5)$$

where $T_a$ (°C) and $P_a$ (Pa) represent the temperature and pressure of the gas mixture, $M_{air}$ and $M_{TCE}$ (g mol$^{-1}$) are the molar masses of the uncontaminated soil air and of the TCE, respectively, and $V_{air}$ and $V_{TCE}$ (m$^3$ mol$^{-1}$) represent the molar volume of the TCE-free soil air and of the TCE.

To express the relative gas permeability, the Campbell-Mualem formulation introduced by Tuli et al. (2005) combined with the equivalence of the Van Genuchten parameter $m$ and the Brooks-Corey parameter $\lambda$ given by Morel-Seytoux et al. (1996) was used:

$$k_{ra} = (1 - \bar{S}_w)^{a_a}\left[1 - \bar{S}_w^{1/m}\right]^2 \quad (6)$$

where $S_w$ (−) is the effective water saturation of the porous medium and $a_a$ denotes the tortuosity-connectivity parameter for gas flow in the porous medium. In our study, we set $a_a$ equal to 0.5 (Marzougui-Jaafar 2013).

According to Thomson et al. (1997), when the compressibility term is neglected, the density of the gas mixture can be expressed as follows:

$$\rho_a = 10^{-6}C_a\left(1 - \frac{M_{air}}{M_{TCE}}\right) + \rho_{air} \quad (7)$$

In a similar way, the dynamic gas viscosity $\mu_a$ was expressed using a linear approximation between the fresh air viscosity and the TCE saturated air viscosity.

The pneumatic head ($H_a^*$) was obtained using the equation (Lusczynski 1960; Mendoza and Frind 1990)

$$H_a^* \equiv z + \frac{P_a}{\rho_{air}g} = \frac{P_m}{\rho_{air}g} \quad (8)$$

where $P_m$ (Pa) is the driving pressure of the gas mixture.

Numerical values of the physical and chemical properties of the TCE and the fine sand are given in Table 2.

The vertical TCE vapour concentration gradients near the soil surface were estimated from the difference between the measured TCE vapour concentration at a soil depth of 0.2 m and the TCE vapour concentration at the soil surface. Because the TCE vapour concentrations measured 5 cm above the soil surface were several orders of magnitude lower than those measured at a depth of 0.2 m, we neglected the TCE concentration at the soil surface when calculating the vertical TCE vapour concentration gradient. The INNOVA photoacoustic device was used to measure the soil TCE concentrations. Because there was no pressure probe available at a depth of 0.2 m, the pressure gradients of

Table 2 Physical and chemical properties of trichloroethylene at 20 °C and properties of the fine-grained sand

| Property | Value | Reference |
|---|---|---|
| TCE | | |
| Density $\rho$ [kg m$^{-3}$] | 1.46 | Dridi 2006 |
| Molar mass $M_{TCE}$ [g mol$^{-1}$] | 131.39 | – |
| Molar volume $V_{TCE}$ [m$^3$ mol$^{-1}$] | 9.4×10$^{-5}$ | Reid et al. 1977 |
| Saturated vapour viscosity $\mu_{a,\,sat}$ [Pa s] | 1.7×10$^{-5}$ | Cotel 2008 |
| Saturated vapour concentration $C_{a,\,sat}$ [kg m$^{-3}$] | 0.42 | Ideal gas law |
| Sand | | |
| Total porosity $\varepsilon$ [–] | 0.43 | Dridi 2006 |
| van Genuchten parameter $m$ [–] | 0.92 | Dridi 2006 |
| Intrinsic permeability $k^*$ [m$^2$] | 5.1×10$^{-12}$ | Dridi 2006 |

the soil gas were quantified from the measured values obtained between pressure probes installed at a depth of 0.25 m and at the soil surface, except for the gas sampling point GM1, where no pressure probe was installed. Because there was no measurement of water saturation available at the soil surface and at a depth of 0.2 m, water saturation measured at a depth of 0.15 m was considered to be representative in all our predictions of vertical TCE vapour fluxes.

Note that using the quasi-analytical approach to evaluate the TCE vapour flux at the soil-air interface is even more accurate when the steady state of the pollutant vapour plume near the soil surface is reached.

During the TCE vapour migration experiment conducted in 2011, both the transient and the steady-state transport conditions of the vapour plume were studied. The TCE vapour concentrations (see Sect. 3.1) and the TCE vapour fluxes from the soil to the atmosphere (see Sect. 3.2) were monitored. In the TCE vapour experiment of 2012, the main goal was to study the steady-state vapour plume to compare the TCE vapour fluxes measured using the various flux chambers at various operation modes (see Sect. 3.3).

# 3 Results and discussion

## 3.1 Fate of the TCE vapour plume

The TCE vapour concentrations were monitored at points GM1, GL and GA1 at various depths, and the water saturation was measured along profiles S1 and S2, where capacitive probes were already installed (see Fig. 1). Figures 2a–c and 3 show the vertical TCE vapour concentration profiles and water saturation profiles at the three monitoring points at five times: at the beginning of the experiment (day 0), at day 5, at day 30 (before raising the water table), at day 31 (just after raising the water table) and at day 33 (just after lowering the water table). Furthermore, Fig. 2d shows the detailed TCE vapour concentration at a depth of 0.2 m at the three monitoring points during the first period of the experiment. According to manufacturer data, there is  2.5 % uncertainty (including the range drift during the experiment) in concentration measurements using the INNOVA photo-acoustic device. There is  3.4 % uncertainty in water saturation measurement using the Sentek EnviroSMART sensors. Because uncertainties in high concentration and water saturation values are slightly

larger than the corresponding symbols used in the graphs, it was difficult to depict them in Figs. 2 and 3.

During the first 30 days after creation of the source zone, the measured TCE vapour concentrations increased with time at all sampling points. This trend was due to the development of the TCE vapour plume from the source zone. At a depth of 0.2 m, the TCE vapour concentration increased over 30 days at GA1 and GL, whereas at GM1, the increase began to diminish strongly 14 days after the TCE injection. Between day 20 and day 26 (inclusive), the average daily increase in TCE vapour concentrations was 3.1 % at sampling point GA1 and 14.2 % at GL. Between day 14 and day 26 (inclusive), however, it was 0.4 % at sampling point GM1, indicating that steady-state vapour transport had already been reached at GM1 at day 14 but had not yet been reached at sampling points GA1 and GL, even before raising of the water table (at day 30). The raising of the water table caused a general significant increase in TCE concentrations in the soil. The upward movement of the water table induces a driving pressure in the soil air resulting in an advective vertical mass flux of high vapour concentrations toward the soil surface. During the lowering of the water table, however, the TCE vapour concentrations decrease because the downward-oriented gradient of the driving pressure in the soil air caused an air flow with low TCE vapour concentration from the soil surface to extend deeper into the soil, thereby diluting the initial high vapour concentrations. These temporal variations caused by the water table fluctuations were greater in the soil in the upper 40 cm (Fig. 2a–c).

From the first days after creation of the TCE source zone, the concentrations observed at the three monitoring points were much higher at depth than those observed near the soil surface. During steady-state transport conditions, the TCE vapour concentrations measured at depths of 0.9 and 0.2 m were, respectively, 19 and 5.1 g m$^{-3}$ at GM1, 31 and 1.4 g m$^{-3}$ at GL and 34 and 1.3 g m$^{-3}$ at GA1. The preferential migration of TCE vapours from the source zone toward the saturated zone was due not only to density-driven advection but also due to molecular diffusion, which was greater downward than upward. Indeed, the water content was much higher in the fine sand layer than in the underlying medium sand (Fig. 3a), thereby resulting in an effective gaseous diffusion coefficient that was lower in the surface sand layer than elsewhere. For example, the mean effective gas diffusion coefficient obtained from Eq. (4) was $1.1 \times 10^{-7}$ m$^2$ s$^{-1}$ at $z = -0.45$ m and $1.5 \times 10^{-6}$ m$^2$ s$^{-1}$ at $z = -0.55$ m.
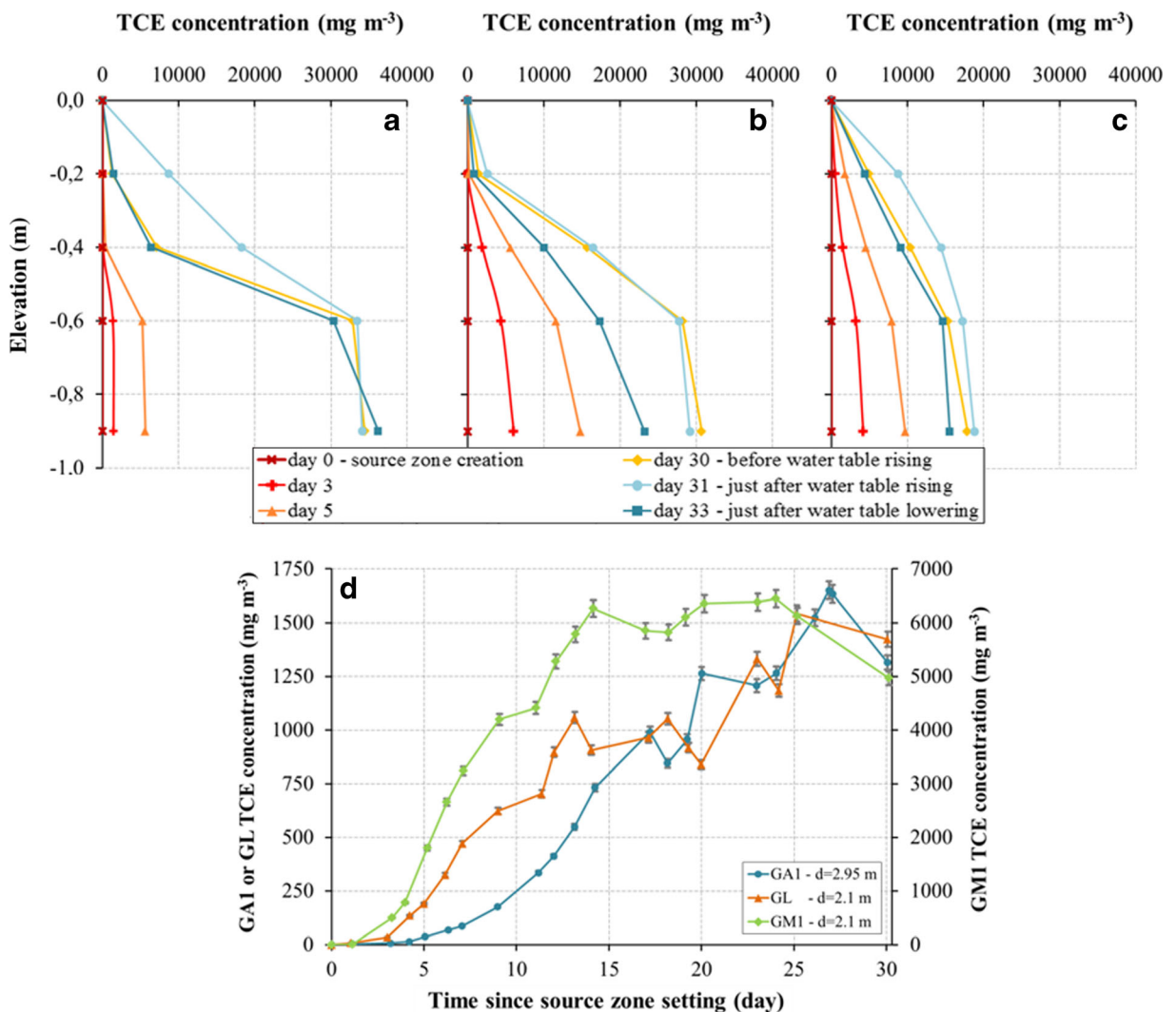
**Fig. 2** TCE vapour concentrations measured at sampling points: TCE vapour profiles at **a** GA1, **b** GL, **c** GM1 and **d** TCE vapour concentrations at GA1, GL and GM1 at a depth of 0.2 m as function of time

Just before raising of the water table, the shape of the vertical profile of TCE vapour concentrations measured at GL and GA1 were similar. Down to a depth of 0.2 m, the concentration gradient was low: 7.1 g m$^{-4}$ at GL and 6.6 g m$^{-4}$ at GA1. The concentration gradients observed between depths of 0.2 and 0.9 m were much greater; for example, at GL and GA1, the mean gradients were approximately 47 and 54 g m$^{-4}$, respectively. At sampling point GM1, the observed vertical TCE concentration profiles differed from those at GL and GA1. Here, the gradients were high and relatively constant between the soil surface and at a depth of 0.6 m, with a mean value of approximately 26 g m$^{-4}$, and very low between depths of 0.6 and 0.9 m, with a mean value of

approximately 9 g m$^{-4}$. This distribution may be explained by the presence of one of the two low-permeability block inclusions located upstream of the monitoring point (see Fig. 1). The observed high water content between depths of 0.8 and 1.45 m (Fig. 3b) significantly reduced the effective gaseous diffusion coefficients in this area and thus hindered the upstream diffusive transport of the vapour plume. Because the vertical diffusive vapour flux at GM1 was greater than at GL and GA1, the TCE vapour concentrations observed near the soil surface in the upper fine sand layer at this sampling point were therefore also greater.

Conversely, just before raising of the water table, the TCE vapour concentrations measured at depths below
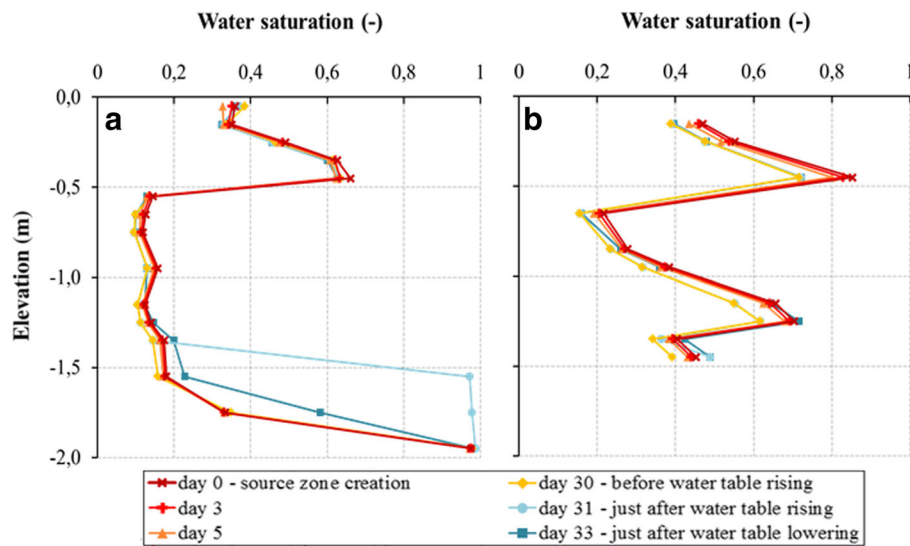
**Fig. 3** Water saturation profiles measured with capacity probes **a** S2, profile without low-permeability blocks, and **b** S1, profile across the upper of the two low-permeability blocks

0.6 m were generally greater at GA1 and GL than at GM1. In fact, GA1 and GM1 were, respectively, located downstream and upstream of the source zone. However, once reaching the groundwater, the low solubility and high density of the TCE vapours caused advective vapour flux toward the capillary fringe of the aquifer and in the flow direction of the groundwater. The TCE vapour concentrations were therefore greater at GA1 than at GM1. At GL, which was located laterally and slightly downstream of the source zone, the measured TCE vapour concentrations were thus between those of GM1 and GA1.

In Sect. 3.2.2, the vertical profiles of both the concentration and water content are used in the evaluation of the TCE vapour flux based on the quasi-analytical method.

## 3.2 TCE vapour fluxes at the soil surface

TCE vapour fluxes from the soil to the atmosphere were monitored in two ways at sampling points GM1, GL and GA1: using measurements at the soil-air interface using flux chambers (Sect. 3.2.1) and using the quasi-analytical approach (Sect. 3.2.2).

### 3.2.1 Measured fluxes using a flux chamber

The TCE vapour fluxes were monitored at the soil-air interface with flux chamber CF3. This flux measurement involved no vapour accumulation in the chamber (see flux measurement method (iii), Eq. (2)). TCE concentrations in

the chambers were measured using the INNOVA photoacoustic device. During the large-scale experiment, approximately 20 TCE vapour flux measurements were performed at GA1, 12 at GL and 16 at GM1 (Fig. 4). These measurements included gas sampling during the raising and lowering of the water table, except at GL, where no measurement was performed during the raising step (Fig. 4). At the same time, the water table level was measured in piezometer P4. Uncertainty in the water level measurement was assumed to be equal to 0.002 m, and uncertainties in the measured TCE mass fluxes could be estimated within the range of 8.8 and 10.5 % using a total derivative expansion for correlated variables (details are presented in the Appendix A).

The TCE vapour flux observed at GM1 was still much greater than the values observed at GA1 and GL which were in the same order of magnitude. This finding is directly linked to the measured TCE concentration gradient observed near the soil surface, which was high at GM1 and similarly low at GA1 and GL (see Fig. 2a–c).

At all sampling points, before raising of the water table, the TCE vapour fluxes increased rapidly during the first time period due to the expansion of the vapour plume. Then, the increases in mass fluxes slowed weakly or gradually depending on the sampling point location when the TCE vapour concentration approached the steady-state transport condition. Between day 17 and day 28 (inclusive), the mean daily increase in TCE vapour flux was approximately 13 % at sampling point GA1 and

**Fig. 4** Water table level monitored in P4 and TCE vapour fluxes measured at sampling points GA1, GL and GM1
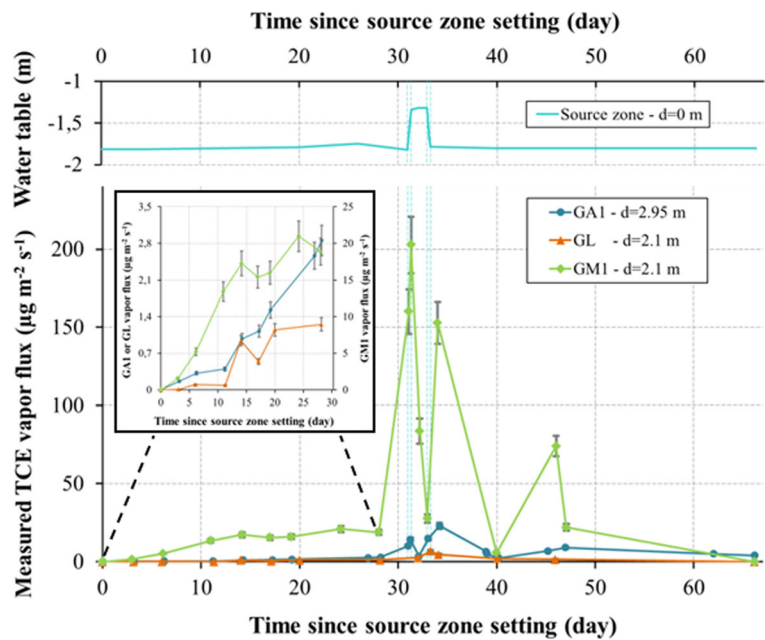


9.7 % at sampling point GL, whereas between day 14 and day 28 (inclusive), it was approximately 1.6 % at sampling point GM1. This finding clearly indicates that the steady state of the vapour plume had already been reached at GM1 at day 14 but had not been completely achieved at sampling points GA1 and GL before raising of the water table. This observation is consistent with the state of the plume indicated by the follow-up of the TCE vapour concentrations monitored near the soil surface soil at each of the three sampling points (see Fig. 2d).

The raising of the water table contributed to a high increase in TCE vapour fluxes: nearly ten and four times the initial fluxes at GM1 and GA1, respectively. This increase can be explained by the substantial increase in TCE vapour concentrations in the unsaturated zone near the soil surface due to upward advective flux induced by driving pressure (see Fig. 2a–c). After stabilisation of the water table, once the driving pressure of the soil air reached its initial equilibrium state, the TCE vapour flux decreased strongly. Over 20 h, the TCE vapour flux decreased by 75 % at GA1 and by 59 % at GM1. Rebalancing of the vapour profile of TCE in the unsaturated zone, i.e., between the atmospheric air slightly charged by TCE vapours and the strong TCE vapour concentrations in the lower part of the vadose zone, caused rapid depletion of the first layers of the soil air near the soil surface, which resulted in very low TCE vapour fluxes. For example, at a depth of 0.2 m, a comparison of the TCE vapour concentrations at the end of

the raising step with those 19 h afterward indicates decreases of 29 % at GA1 and 56 % at GM1.

Conversely, lowering of the water table should cause a decrease in TCE vapour fluxes at the soil surface because the TCE vapour concentrations measured near the soil surface decrease (see Fig. 2a–c) due to downward advective fluxes induced by the driving pressure gradient and dilution by atmospheric air with low TCE vapour concentration from the soil surface. However, this pattern was present only at GM1, where there was a decrease in the vapour flux of approximately 67 %. At GA1 and GL, the vapour fluxes increased by as much as 310 and 170 %, respectively. This unexpected result was most likely due to a strong increase in the soil temperature during the lowering step. Note that the temperature at the soil surface increased from an average of 18.9 to 26.8 °C during flux measurements at sampling points GL and GA1. However, at sampling point GM1, the temperature decreased from 21.6 to 16.7 °C during the measurements. A temperature increase is usually accompanied with an increase in both the molecular diffusion coefficient of TCE vapours and the TCE saturation concentration in the gas phase near the source zone (Cotel 2008). Note that in the present study of flux measurements, only the indirect effects of water table raising and lowering, such as the modified distribution of TCE vapour concentration in the unsaturated zone, were taken into account; the closed flux chambers did not allow for any measurements of advective vapour fluxes.

Once the water level reached its initial state, two peaks of TCE vapour fluxes were particularly evident at GM1 and GA1 on day 34 and day 46. The first peak was likely caused by the replacement of the concrete slab by a more-permeable one; the second peak resulted from additional flux chamber tests (see Sect. 2.2). The removal of the concrete slab most likely caused a suction of highly concentrated TCE vapours from deeper soil horizons to the soil surface and thus contributed to an increase in diffusive fluxes of TCE vapour at the soil-air interface. The additional flux chamber tests conducted between day 43 and day 47 may have also strongly disturbed the TCE vapour plume in the vadose zone near the soil surface.

### 3.2.2 Estimated fluxes using the quasi-analytical approach

TCE vapour fluxes were calculated using Eq. (3). Uncertainties of approximately 16.5 and 16.1 % in the diffusive and advective portions, respectively, of the predicted fluxes were estimated based on the total derivative expansions for correlated variables (for details, see Appendix B).

Figure 5 presents the diffusive and advective vapour fluxes between a depth of 0.2 m and the soil surface at the three sampling points. The corresponding advective part of mass flux at point GM1 could not be calculated because there was no pressure sensor placed near this sampling point (see Fig. 1).

The calculated vapour fluxes display essentially the same trends as the measured vapour fluxes: the predicted TCE vapour flux at GM1 nearly always exceeded the calculated value at sampling point GA1 or GL. An initial period of increase in diffusive vapour fluxes during the establishment of the TCE vapour plume was followed, on day 31, during the groundwater raising, by a stronger increase in these mass fluxes. At the end of the experiment, the diffusive TCE vapour fluxes diminished greatly due to the depletion of the TCE source zone. However, contrary to the mass fluxes measured at the interface soil/air, the diffusive TCE vapour fluxes calculated using Fick's law strongly decreased in accordance with the expected decrease in vapour flux, on day 33, during the groundwater lowering.

The calculated advective vapour fluxes were very low, apart from the groundwater raising and lowering periods. Advection was therefore only gravitational, and because the TCE vapour concentrations near the soil surface were very low, the advective mass fluxes were also low. Between a depth of 0.2 m and the soil surface, the

maximum ratio between the density-driven advective fluxes and total mass fluxes were 0.47 % at sampling point GA1 and 0.16 % at GL. The density-driven advection was thus negligible during our experiment. During the groundwater raising and lowering, the TCE advective vapour fluxes, which were principally linked to gradients of the driving pressure, were significant although distinctly lower than the diffusive TCE vapour fluxes. Between a depth of 0.2 m and the soil surface, they represented, for example at GA1, approximately 10.8 % of the total flux during the raising stage and 13.6 % of the total flux during the lowering stage. During the raising and lowering, the calculated advective vapour fluxes of TCE were greater in deeper soil horizons than near the soil surface due to the increase in recorded driving pressure gradients with depth.

### 3.2.3 Comparison of measured and calculated TCE vapour fluxes

Figure 6 shows a comparison between mass fluxes measured at the soil/air interface and diffusive fluxes calculated using Fick's law between a depth of 0.2 m and the soil surface at sampling points GA1, GL and GM1.

Before raising of the water table, the TCE vapour fluxes measured at sampling points GA1 and GL were often much lower than the estimated vapour fluxes calculated between a depth of 0.2 m and the soil surface. However, at sampling point GM1, from day 11, the measured and calculated mass fluxes were very close. Indeed, at GM1, the vapour plume had already achieved steady-state transport conditions on day 14, whereas at GA1 or GL, steady-state conditions were not reached even on day 30 (see Sects. 3.1 and 3.2.1). Because steady-state transport had not yet been reached, the TCE gradients near the soil surface were lower than the mean gradient between a depth of 0.2 m and the soil surface. The TCE fluxes measured at the soil-air interface directly related to these low TCE vapour gradients observed near the soil surface were therefore lower than the fluxes calculated using Fick's law and based on a mean gradient between a depth of 0.2 m and the soil surface. In this case, using Fick's first law to assess the TCE vapour flux from the subsurface to the atmosphere caused an overestimation of the diffusive TCE vapour flux, all the more important because the vertical concentration profile was far from its equilibrium state. Only when steady-state transport was reached, the calculated diffusive mass fluxes between a depth of 0.2 m and the soil surface were representative of the diffusive mass fluxes at the soil-air interface (Dridi and Schäfer 2006).
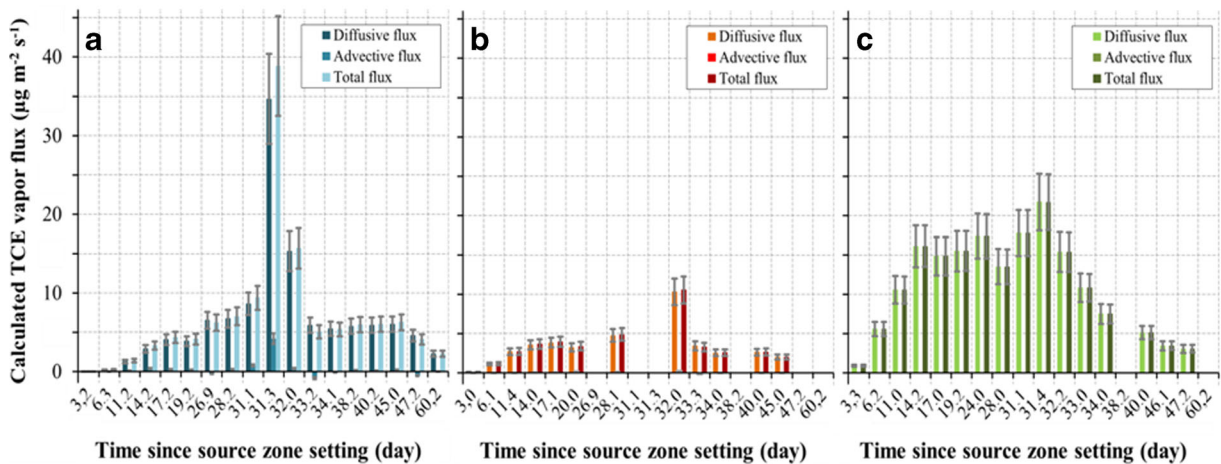
**Fig. 5** Diffusive, advective and total TCE vapour fluxes calculated between a depth of 0.2 m and the soil surface at sampling points **a** GA1, **b** GL and **c** GM1

While the water table was raised, the ratio of the measured vapour flux to the calculated diffusive vapour flux increased greatly. The raising of the water table causes an upward displacement of the TCE vapour plume. This resulted, if a steady state was reached before the water table raising, in TCE vapour gradients near the soil surface much higher than the mean gradient between a depth of 0.2 m and the soil surface, based on

the application of Fick's law. The fluxes measured at the soil-air interface governed by these high vapour gradients near the soil surface were much higher than the diffusive fluxes calculated using Fick's law.

Following the raising of the water table, the fluxes measured at the soil/air interface were significantly affected by a modification of the TCE vapour plume due to both the replacement of the concrete slab and

**Fig. 6** Water table level monitored in P4 and ratio between measured TCE vapour fluxes and calculated diffusive vapour fluxes at points GA1, GL and GM1
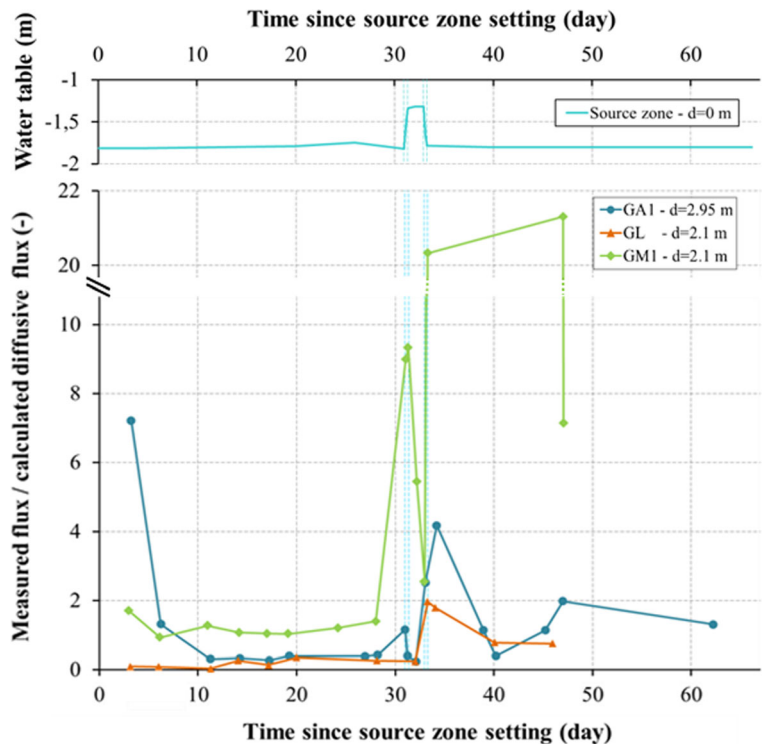
additional testing of flux chambers (see Sect. 3.2.1). Therefore, it is not very relevant to study the ratio of measured and calculated vapour fluxes.

3.3 Comparison of flux measurements using various devices

In the TCE vapour experiment of 2012, on day 35 after creation of the TCE source zone, five flux chamber devices (CF1, CF2, CF3, CF4 and CF5) were successively placed at measurement points GA1, GL and GM1. At each location and for each flux chamber, flux measurements were performed using the three previously described methods. To measure the TCE vapour concentration within the flux chamber, the INNOVA photo-acoustic device was used at GA1, and two portable photo-ionisation detectors were used at GL and GM1. Note that for flux measurement method (iii), the TCE mass adsorbed on the charcoal was additionally analysed (see Sect. 2.3). Using total derivative expansions for correlated variables, estimated uncertainties in measured fluxes were within the range of 9.2 and 34 %, considering, inter alia, uncertainties in the chamber section of 4 % and in the chamber volume of 4 % (CF2, CF3, CF4 and CF5) and uncertainties of 25 % in the net volume of very small flux chamber CF1 (for details, see Appendices A and C).

Figure 7 shows the TCE vapour fluxes measured at the soil/air interface using the various flux chambers at sampling points GA1, GL and GM1. Additionally, for comparison purposes, the diffusive mass fluxes calculated between a depth of 0.2 m and the soil surface using Eq. (3), are also shown in the figure. Uncertainties of

16.5 % in calculated diffusive fluxes were estimated (for details, see Appendix B).

As in the flux measurements of 2011, the TCE vapour fluxes monitored at sampling point GM1 exceeded those measured at GL or GA1. At each sampling point, the vapour fluxes measured using the various flux chambers and the various methods are of the same order of magnitude. The relative variability in measured flow is reasonable, with a standard deviation of 33 % at GA1, 18 % at GM1 and 21 % at GL. The highest relative variability in fluxes measured at GA1 can be explained by the lower values of flux at this point, which made their measurement more difficult.

As in the campaign of 2011, the measured fluxes were similar to the diffusive fluxes calculated at GM1 and much lower at GA1, which may be explained by the steady-state condition of the vapour plume that had already been reached at sampling point GM1 but not at GA1. Contrary to what was observed in 2011, the mass fluxes measured at GL in 2012 were similar to the calculated diffusive mass fluxes. This pattern could be explained by the larger volume of TCE used to create the source zone and the delayed flux measurements, which left more time for development of steady-state conditions of the near-surface TCE vapour plume.

Figure 8 shows the TCE vapour fluxes measured using the various flux chambers and flux measurement methods compared to the calculated diffusive fluxes. Table 3 summarises the average flux measured using each flux chamber and method.

The geometry of the flux chamber did not have a significant effect on the TCE vapour flux measured at
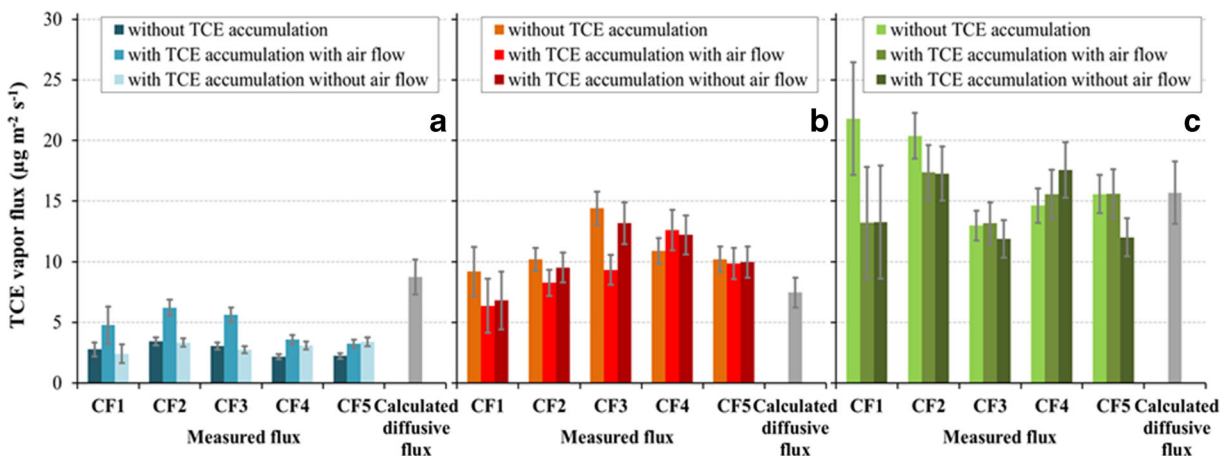


**Fig. 7** TCE vapour fluxes measured at sampling points **a** GA1, **b** GL and **c** GM1 with various flux chambers and diffusive fluxes calculated between a depth of 0.2 m and the soil surface
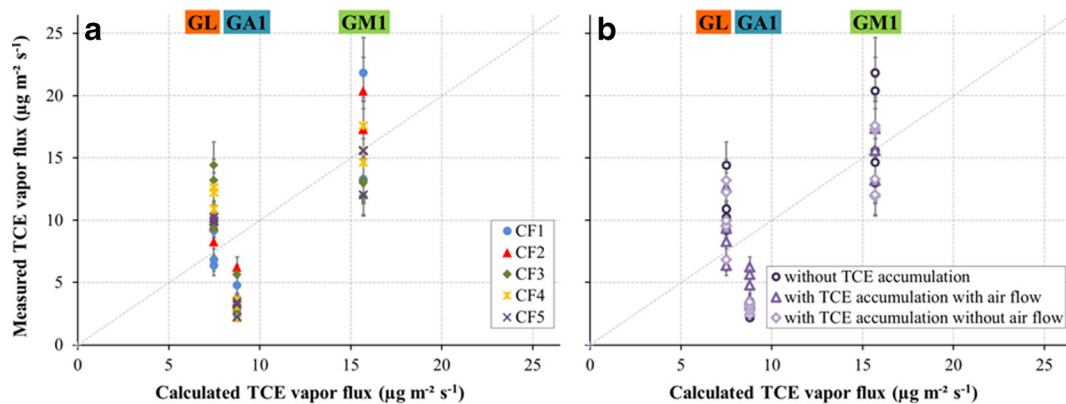
**Fig. 8** TCE vapour fluxes measured at sampling points GA1, GL and GM1 highlighting the use of **a** various flux chambers and **b** various flux measurement methods and compared to calculated diffusive TCE vapour fluxes

the scale of the SCERES facility (Fig. 8a). There was no flux chamber associated with systematically higher or lower vapour fluxes than the others. The lowest fluxes at measuring points GA1, GL and GM1 were obtained with flux chambers CF4, CF1 and CF3, respectively. The highest fluxes at measuring points GA1, GL and GM1 were observed with flux chambers CF2, CF3 and CF1, respectively. The impact of the geometry of the chamber on the measured vapour fluxes was quite low with the measured mean fluxes, regardless of the method of measurement: between 2.9 and 4.3 $\mu g\ m^{-2}\ s^{-1}$ at GA1, between 7.5 and 12.3 $\mu g\ m^{-2}\ s^{-1}$ at GL and between 12.7 and 18.3 $\mu g\ m^{-2}\ s^{-1}$ at GM1 (Table 3). However, vapour fluxes measured with certain flux chambers were often either very close to the average flux measured at a sampling point or far away. Low deviations from the averages of 8 and 13 % were obtained with flux chambers CF4 and CF5. High deviations from the average of approximately 18, 25 and 27 %, were obtained using CF2, CF3 and CF1, respectively. The high deviations in the case of CF2 and CF3 can be explained by the higher vapour fluxes measured in accumulation and recirculation mode at sampling point GA1 (see Fig. 7). However, only three locations were used for the comparison of the measured vapour fluxes with the various methods. The only flux chamber that may have had a less appropriate geometry appears to be CF1. Even if the results do not differ significantly from those obtained with the other flux chambers, its small height and volume may have caused large uncertainties in the estimation of measured fluxes.

The effect of the measuring method on the monitored TCE vapour fluxes was also low (Fig. 8b). Regardless of the flux chamber used, the mean fluxes varied between

2.7 and 4.7 $\mu g\ m^{-2}\ s^{-1}$ at GA1, between 9.3 and 11.0 $\mu g\ m^{-2}\ s^{-1}$ at GL and between 14.4 and 17.1 $\mu g\ m^{-2}\ s^{-1}$ at GM1 (see Table 3). The vapour fluxes did not display a general pattern associated with the measuring method. For example at sampling points GL and GM1, the measuring method without TCE vapour accumulation in the chamber nearly always yielded higher vapour fluxes than the two other methods, whereas at sampling point GA1, the same measuring method yielded the lowest vapour fluxes in each flux chamber. On average, the vapour fluxes measured at GL and GM1 without accumulation were, respectively 15 and 17 % higher than the mean flux measured using the accumulation methods. However, at sampling point GA1, it was 29 % lower than those obtained with the accumulation methods. Unlike many other studies (e.g., Gao and Yates 1998; Davidson et al. 2002; Pumpanen et al. 2004), we did not observe a significant general underestimation of the measured TCE vapour fluxes using the methods with vapour accumulation in the chamber headspace. There may be various explanation for this finding: (i) the volume of the flux chambers was rather large for typical static or closed dynamic chambers, thereby causing a dilution of vapour concentration in the chamber headspace (Hudson and Ayoko 2008); (ii) the time interval used for the flux measurement was relatively short in accordance with recommendations for the use of flux chambers with accumulation of vapour in the chamber headspace (e.g., Gao and Yates 1998; Davidson et al. 2002; Hudson and Ayoko 2008; Rochette 2011); and (iii) the chosen flow rate of air recirculation used in the method without TCE accumulation was too low to efficiently avoid the vapour accumulation in the flux chamber

**Table 3**  Mean fluxes measured (with standard deviation) using the various flux chambers and methods

| Measuring point | Average on the fluxes measured with the three flux measurement methods ($\mu g\ m^{-2}\ s^{-1}$) | | | | | Average on the fluxes measured with the five flux chambers ($\mu g\ m^{-2}\ s^{-1}$) | | |
|---|---|---|---|---|---|---|---|---|
| | Flux chamber | | | | | Flux measurement method | | |
| | CF1 | CF2 | CF3 | CF4 | CF5 | Method (i)[a] | Method (ii)[b] | Method (iii)[c] |
| GA1 | 3.3  1.0 | 4.3  1.3 | 3.8  1.3 | 2.9  0.6 | 3.0  0.5 | 3.0  0.4 | 4.7  1.2 | 2.7  0.5 |
| GL | 7.5  1.2 | 9.3  0.8 | 12.3  2.2 | 11.9  0.7 | 10.0  0.1 | 10.3  2.2 | 9.3  2.0 | 11.0  2.0 |
| GM1 | 16.1  4.0 | 18.3  1.5 | 12.7  0.6 | 15.9  1.2 | 14.4  1.7 | 14.4  2.5 | 15.0  1.6 | 17.1  3.4 |

[a] With TCE vapour accumulation without air recirculation

[b] With TCE vapour accumulation with air recirculation at a low flow rate

[c] Without TCE vapour accumulation in the chamber

headspace. Note that the preliminary measurements of TCE vapour flux using flux chamber CF3 and an air flow rate of 1 L min$^{-1}$ caused a driving pressure difference between the air inside the chamber and the atmospheric air that exceeded the desired maximum pressure difference of 1 Pa.

Furthermore, based on a comparison of the vapour fluxes measured with the accumulation methods, the effect of the air recirculation was not significant. For example, the vapour fluxes obtained at GA1 and GM1 with air recirculation often resulted in the highest mass fluxes, whereas at GL they were often lowest (see Fig. 8b). The vapour fluxes measured with air recirculation in the chamber were 41 and 5 % higher at GA1 and GM1, respectively, and 10 % lower at GL than those obtained without air recirculation. We did not observe a significant effect of the mixing fan in flux chambers CF2 and CF4 on the measured TCE vapour flux. Our findings do not favour any one of the three fluxes measuring methods; the three methods yielded vapour fluxes with similar averages and variances. Using the measuring method without vapour accumulation in the chamber, however, has the advantage of monitoring of the mass flux under more natural transfer conditions at the soil-air interface. Indeed in field sites, pollutant vapour concentration in the atmospheric air near the soil surface is in general very low due to the instantaneous dilution of TCE vapours emanating from the vadose zone by the lateral wind.

## 4 Conclusions

Based on controlled TCE vapour plume experiments performed on the large-scale artificial aquifer SCERES,

TCE vapour fluxes at the soil surface were experimentally quantified using various flux chambers and operational modes under both transient and steady-state conditions of the vapour plume and using a quasi-analytical approach based on soil gas measurements.

Upward displacement of the water-air front during the controlled raising of the water table increased the TCE vapour fluxes measured at the soil surface by factors of 4 to 10. At steady-state transport conditions, TCE vapour fluxes measured with the flux chambers and estimated using the quasi-analytical approach were of the same order of magnitude aside from a few discrepancies. In the case where the steady-state of transport of the vapour concentration was not yet reached, the TCE vapour flux predicted by the quasi-analytical approach can greatly underestimate or overestimate the real TCE vapour flux at the soil-air interface, depending on the level of instationnarity of TCE vapour concentrations in the vadose zone. This highlights the importance of steady-state conditions of the DNAPL vapour plume near the soil surface when using the quasi-analytical approach. It was also concluded that the advective portion of TCE vapour fluxes at the soil surface of the artificial porous aquifer is relatively low compared to the diffusive portion, even during the experimental step of sequentially raising and lowering the water table. The calculated advective flux remained lower than 15 % of the total mass flux during all our experimentation. Neglecting the advective vapour flux, as is the case when using closed flux chambers, will thus not contribute to large errors in estimation of the total TCE vapour flux at the soil surface. At field sites, when diffusion processes are less dominant than in the studied experimental setup, this might not always be the case.

The three flux measurement methods using five types of closed flux chambers yielded similar results. It was shown that the effects of both the accumulation of TCE vapours in the flux chamber and the mixing fan on the measured TCE vapour fluxes are low. These results do not completely agree with certain previous findings (Gao and Yates 1998; Davidson et al. 2002; Pumpanen et al. 2004; Hudson and Ayoko 2008). Furthermore, the experiments do not favour any one of the three measuring methods; the three methods yielded vapour fluxes with similar averages and variances. Nevertheless, air recirculation at a low flow rate combined with a charcoal trap generally has two major advantages: limiting vapour accumulation in the flux chamber and quantifying the individual mass fluxes in a multicomponent system. The latter is of practical interest in actual cases of site contamination.

The study highlighted methodological aspects of and uncertainties in the evaluation of VOC vapour fluxes at the soil surface under both transient and steady-state conditions of the vapour plume. It thus helps to accurately predicting the environmental impact of organic pollution of contaminated sites in terms of vapour fluxes from the subsurface to the building or atmosphere.

# Appendices

## Appendix A Uncertainties in the experimental TCE mass fluxes measured without TCE vapour accumulation in the flux chamber (see Eq. (2))

Uncertainties in the TCE mass fluxes were determined using a total derivative expansion for correlated variables of $F_{soil/atm}$:

$$\frac{\Delta F_{soil/atm}}{F_{soil/atm}} = \frac{\Delta m_{ads} + V_{ch}\Delta C_{ch} + C_{ch}\Delta V_{ch}}{m_{ads} + C_{ch}V_{ch}} + \frac{\Delta A_{ch}}{A_{ch}} + \frac{\Delta(\Delta t)}{\Delta t} \quad (9)$$

Here, $\Delta m_{ads}$ and $\Delta C_{ch}$ are the errors in the fixed TCE mass and residual vapour concentration in the chamber. In addition, $\Delta V_{ch}$, $\Delta A_{ch}$ and $\Delta(\Delta t)$ are the net volume, measured area and time measuring interval

errors, respectively. By neglecting errors in time recording and assuming relative uncertainties of 4 % in the sorbed TCE mass (gas chromatography analysis), 2.5 % in the TCE vapour concentration (INNOVA measurements) or 5 % (photo-ionisation detectors measurements), 4 % in the chamber section and chamber volume (CF2, CF3, CF4 and CF5) and 25 % in the net volume of very small flux chamber CF1, relative uncertainty in the pollutant vapour flux measured without TCE vapour accumulation in the flux chamber can be determined.

For Sect. 3.2.1, relative uncertainties in the flux were within the range of 8.8 and 10.5 %.

For Sect. 3.3, relative uncertainties in the flux were within the range of 9.2 and 23.1 %.

## Appendix B Uncertainties in the calculated TCE mass fluxes using the quasi-analytical approach (see Eq. (3))

Uncertainties in the diffusive portion of the predicted TCE vapour fluxes were determined using the equation

$$\frac{\Delta F_{diff,z}}{F_{diff,z}} = \frac{10}{3}\frac{\Delta S_a}{S_a} + \frac{4}{3}\frac{\Delta\varepsilon}{\varepsilon} + \frac{\Delta(dC_a/dz)}{dC_a/dz} \quad (10)$$

which follows from Eq. (3) using a total derivative expansion for correlated variables. Considering uncertainties of 3.4 % in the gas saturation measurements ($\Delta S_a/S_a$), 2 % in the sand porosity ($\Delta\varepsilon/\varepsilon$) and 2.5 % in the vapour concentration gradients ($\Delta(dC_a/dz)/(dC_a/dz)$) based on the INNOVA measurements and assuming no errors in the free air diffusion coefficient, a total uncertainty in the predicted diffusive vapour flux of approximately 16.5 % was obtained.

In a similar way, assuming no error in the estimation of the density of the uncontaminated soil air and in the dynamic gas viscosity and neglecting error in the relative gas pressure (manufacturer data yield a relative uncertainty of 0.1 %), uncertainties in the advective portion of the estimated TCE vapour fluxes were determined using the equation

$$\frac{\Delta F_{conv,z}}{F_{conv,z}} = \frac{\Delta C_a}{C_a} + \frac{\Delta k_{ra}}{k_{ra}} + \frac{\Delta k^*}{k^*} + \frac{\Delta\rho_a}{\rho_a} \quad (11)$$

with $\dfrac{\Delta k_{ra}}{k_{ra}} = \left(a_a + \dfrac{2}{m}\right)\dfrac{\Delta S_w}{S_w}$ and $\dfrac{\Delta\rho_a}{\rho_a} = \dfrac{\Delta C_a}{C_a}$

Considering uncertainties of 2.5 % in the vapour concentrations ($\Delta C_a/C_a$) based on the INNOVA measurements, 3.4 % in the water saturation measurements ($\Delta S_w/S_w$) and 2 % in the sand permeability ($\Delta k^*/k^*$), a total uncertainty of 16.1 % in the predicted advective vapour flux was obtained.

## Appendix C Uncertainties in the experimental TCE mass fluxes measured with TCE vapour accumulation in the flux chamber (see Eq. (1))

Uncertainties in the TCE mass fluxes were determined using a total derivative expansion for correlated variables of $F_{soil/atm}$:

$$\frac{\Delta F_{soil/atm}}{F_{soil/atm}} = \frac{\Delta(dC_{ch}/dt)}{dC_{ch}/dt} + \frac{\Delta V_{ch}}{V_{ch}} + \frac{\Delta A_{ch}}{A_{ch}} \quad (12)$$

Considering uncertainties of 2.5 % in the temporal TCE concentration variation ($\Delta(dC_{ch}/dt)/(dC_{ch}/dt)$) (INNOVA measurements) or 5 % (photo-ionisation detectors measurements), uncertainties in the chamber section of 4 % and in the chamber volume of 4 % (CF2, CF3, CF4 and CF5) and uncertainties of 25 % in the net volume of very small flux chamber CF1, the total uncertainty in the measured fluxes with TCE vapour accumulation in the flux chamber ranged between 10.5 and 34 %.

## References

Altevogt, A. S., Rolston, D. E., & Venterea, R. T. (2003). Density and pressure effects on the transport of gas phase chemicals in unsaturated porous media. *Water Resources Research, 39*, 1061–1071.

Baehr, A. L., & Bruell, C. J. (1990). Application of the Stefan-Maxwell equations to determine limitations of Fick's law when modeling organic vapor transport in sand columns. *Water Resources Research, 26*, 1155–1163.

Bahr, D. E., Aldrich, T. E., Seidu, D., Brion, G. M., Tollerud, D. J., & Paducah Gaseous Diffusion Plant Project Team et al. (2011). Occupational exposure to trichloroethylene and cancer risk for workers at the Paducah Gaseous Diffusion Plant. *International Journal of Occupational Medicine and Environmental Health, 24*, 67–77.

Batterman, S. A., McQuown, B. C., Murthy, P. N., & McFarland, A. R. (1992). Design and evaluation of a long-term soil gas flux sampler. *Environmental Science & Technology, 26*, 709–714.

Bekku, Y., Koizumi, H., Nakadai, T., & Iwaki, H. (1995). Measurement of soil respiration using closed chamber method: an IRGA technique. *Ecological Research, 10*, 369–373.

Bohy, M., Dridi, L., Schäfer, G., & Razakarisoa, O. (2006). Transport of a mixture of chlorinated solvent vapors in the vadose zone of a sandy aquifer. *Vadose Zone Journal, 5*, 539–553.

Carpi, A., Fostier, A. H., Orta, O. R., dos Santos, J. C., & Gittings, M. (2014). Gaseous mercury emissions from soil following forest loss and land use changes: field experiments in the United States and Brazil. *Atmospheric Environment, 96*, 423–429.

Choi, J. W., Tillman, F. D., & Smith, J. A. (2002). Relative importance of gasphase diffusive and advective trichloroethylene fluxes in the unsaturated zone under natural conditions. *Environmental Science & Technology, 36*, 3157–3164.

Christiansen, J. R., Korhonen, J. F. J., Juszczak, R., Giebels, M., & Pihlatie, M. (2011). Assessing the effects of chamber placement, manual sampling and headspace mixing on CH4 fluxes in a laboratory experiment. *Plant Soil, 343*, 171–185.

Collier, S. M., Ruark, M. D., Oates, L. G., Jokela, W. E., & Dell, C. J. (2014). Measurement of greenhouse gas flux from agricultural soils using static chambers. *Journal of Visualized Experiments, 90*, e52110.

Cotel, S. (2008). *Etude des transfers sol/nappe/atmosph re/bâtiments ; Application aux sols pollu s par des Compos s Organiques Volatils*. Th se de doctorat de l'Universit Joseph Fourier de Grenoble.

Cotel, S., Schäfer, G., Barthes, V., & Baussand, P. (2011). Effect of density-driven advection on trichloroethylene vapor diffusion in a porous medium. *Vadose Zone Journal, 10*, 565–581.

Davidson, E. A., Savage, K., Verchot, L. V., & Navarro, R. (2002). Minimizing artifacts and biases in chamber-based measurements of soil respiration. *Agricultural and Forest Meteorology, 113*, 21–37.

Di Francesco, F., Ferrara, R., & Mazzolai, B. (1998). Two ways of using a chamber for mercury flux measurement—a simple mathematical approach. *Science of the Total Environment, 213*, 33–41.

Dridi, L. (2006). *Transfert d'un m lange de solvants chlor s en aquif re poreux h t rog ne: exp rimentations sur site contrôl et simulations num riques*. Th se de doctorat de l'Universit Louis Pasteur de Strasbourg.

Dridi, L., & Schäfer, G. (2006). Quantification du flux de vapeurs de solvants chlor s depuis une source en aquif re poreux vers l'atmosph re: biais relatifs à la non uniformit de la teneur en eau et à la non stationnarit du transfert. *Comptes Rendus M canique, 334*, 611–620.

Dridi, L., Pollet, I., Razakarisoa, O., & Schäfer, G. (2009). Characterisation of a DNAPL source zone in a porous aquifer using the Partitioning Interwell Tracer Test and an inverse modelling approach. *Journal of Contaminant Hydrology, 107*, 22–44.

Baker, K., Berry, D., Christmann, C., Dellechaie, F., Diaz, T., Gallagher, D., Klein, K., Mingay, M., Parsons, B., Rainey, L., Schum, M., Sorensen, M., Sotelo, J., Stacy, A., & Zanoria, F. (2011). *Guidance for the evaluation and mitigation of subsurface vapor intrusion to indoor Air (vapor intrusion guidance)*. California: Department of Toxic Substances Control, California Environmental Protection Agency.

Eckley, C. S., Gustin, M., Lin, C.-J., Li, X., & Miller, M. B. (2010). The influence of dynamic chamber design and operating parameters on calculated surface-to-air mercury fluxes. *Atmospheric Environment, 44*, 194–203.

Eklund, B., Balfour, W., & Schmidt, C. (1985). Measurement of fugitive volatile organic emission rates. *Environmental Progress, 4*(3), 199–202.

Gallego, E., Perales, J. F., Roca, F. J., & Guardino, X. (2014). Surface emission determination of volatile organic compounds (VOC) from a closed industrial waste landfill using a self-designed static flux chamber. *Science of the Total Environment, 470–471*, 587–599.

Gao, F., & Yates, S. R. (1998). Laboratory study of closed and dynamic flux chambers: experimental results and implications for field application. *Journal of Geophysical Research, 103*, 26115–26125.

Grathwohl, P. (1998). *Diffusion in natural porous media: contaminant transport, sorption/desorption and dissolution kinetics.* Boston, MA: Kluwer Academic Publishers.

Happell, J. D., Mendoza, Y., & Goodwin, K. (2014). A reassessment of the soil sink for atmospheric carbon tetrachloride based upon static flux chamber measurements. *Journal of Atmospheric Chemistry, 71*, 113–123.

Hudson, N., & Ayoko, G. A. (2008). Odour sampling 2: comparison of physical and aerodynamic characteristics of sampling devices: a review. *Bioresource Technology, 99*, 3993–4007.

Jellali, S., Benremita, H., Muntzer, P., Razakarisoa, O., & Schäfer, G. (2003). A large-scale experiment on mass transfer of trichloroethylene from the unsaturated zone of a sandy aquifer to its interfaces. *Journal of Contaminant Hydrology, 60*, 31–53.

Kanemasu, E. T., Powers, W. L., & Sij, J. W. (1974). Field chamber measurements of $CO_2$ flux from soil surface. *Soil Science, 118*, 233–237.

Lenhard, R. J., Oostrom, M., Simmons, C. S., & White, M. D. (1995). Investigation of density-dependent gas advection of trichloroethylene: experiment and a model validation exercise. *Journal of Contaminant Hydrology, 19*, 47–67.

Lerner, D. N., Bourg, A. C. M., Gosk, E., Biscop, P. K., Mouvet, C., Degranges, P., Jakobsen, R., Burston, M. W., & Barberis, D. (1991). Sources et mouvements des solvants chlorés dans les eaux souterraines de Coventry (Grande Bretagne). *Hydrogéologie, 4*, 275–282.

Lindberg, S. E., Zhang, H., Vette, A. F., Gustin, M. S., Barnett, M. O., & Kuiken, T. (2002). Dynamic flux chamber measurement of gaseous mercury emission fluxes over soils. Part 2—effect of flushing flow rate and verification of a two-resistance exchange interface simulation model. *Atmospheric Environment, 36*, 847–859.

Liu, F., Cheng, H., Yang, K., Zhao, C., Liu, Y., Peng, M., & Li, K. (2014). Characteristics and influencing factors of mercury exchange flux between soil and air in Guangzhou City. *Journal of Geochemical Exploration, 139*, 115–121.

Lund, C. P., Riley, W. J., Pierce, L. L., & Field, C. B. (1999). The effects of chamber pressurization on soil-surface $CO_2$ flux and the implications for NEE measurements under elevated $CO_2$. *Global Change Biology, 5*, 269–281.

Lusczynski, N. J. (1960). Head and flow of ground water of variable density. *Journal of Geophysical Research, 66*, 4247–4256.

Massmann, J., & Farrier, D. F. (1992). Effects of atmospheric pressures on gas transport in the vadose zone. *Water Resources Research, 28*(3), 777–791.

Maier, M., & Schack-Kirchner, H. (2014). Using the gradient method to determine soil gas flux: a review. *Agricultural and Forest Meteorology, 192–193*, 78–95.

Ma, M., Wang, D., Sun, R., Shen, Y., & Huang, L. (2013). Gaseous mercury emissions from subtropical forested and open field soils in a national nature reserve, southwest China. *Atmospheric Environment, 64*, 116–123.

Matthias, A. D., Blackmer, A. M., & Bremner, J. M. (1980). A simple chamber technique for field measurement of emissions of nitrous oxide from soils. *Journal of Environmental Quality, 9*, 251–256.

Marzougui, S., Schäfer, G., & Dridi, L. (2012). Prediction of vertical DNAPL vapour fluxes in soils using quasi-analytical approaches: bias related to density-driven and pressure-gradient-induced advection. *Water Air Soil Pollution, 223*, 5817–5840.

Marzougui-Jaafar, S. (2013). *Transfert d'un composé organochloré depuis une zone source localisée en zone non saturée d'un aquifère poreux vers l'interface sol-air : expérimentations et modélisations associées*. Thèse de doctorat de l'Université de Strasbourg

Mendoza, C. A., & Frind, E. O. (1990). Advective-dispersion transport of dense organic vapors in the unsaturated zone, 1-Model development and 2-Sensibility analysis. *Water Resources Research, 26*, 379–398.

Millington, R. J., & Quirk, J. M. (1961). Permeability of porous solids. *Transactions of the Faraday Society, 57*, 1200–1207.

Miola, E. C. C., Aita, C., Rochette, P., Chantigny, M. H., Angers, D. A., Bertrand, N., & Gasser, M.-O. (2015). Static Chamber Measurements of Ammonia Volatilization from Manured Soils: Impact of Deployment Duration and Manure Characteristics. *Soil Science Society of America Journal, 79*, 305–313.

Morel-Seytoux, H. J., Meyer, P. D., Nachabe, M., Touma, J., van Genuchten, M. T., & Lenhard, R. J. (1996). Parameter equivalence for the Brooks-Corey and van Genuchten soil characteristics: Preserving the effective capillary drive. *Water Resources Research, 32*, 2031–2041.

Nay, S. M., Mattson, K. G., & Bormann, B. T. (1994). Biases of chamber methods for measuring soil $CO_2$ efflux demonstrated with a laboratory apparatus. *Ecology, 75*, 2460–2463.

Nômmik, H. (1973). The effect of pellet size on the ammonia loss from urea applied to forest soil. *Plant Soil, 39*, 309–318.

Pankow, J. F., & Cherry, J. A. (1996). *DNAPLs in groundwater: History, behavior and remediation*. Portland, Oregon: Waterloo Press.

Parker, D., Ham, J., Woodbury, B., Cai, L., Spiehs, M., Rhoades, M., Trabue, S., Casey, K., Todd, R., & Cole, A. (2013a). Standardization of flux chamber and wind tunnel flux measurements for quantifying volatile organic compound and ammonia emissions from area sources at animal feeding operations. *Atmospheric Environment, 66*, 72–83.

Parker, D. B., Gilley, J., Woodbury, B., Kim, K.-H., Galvin, G., Bartelt-Hunt, S. L., Li, X., & Snow, D. D. (2013b). Odorous VOC emission following land application of swine manure slurry. *Atmospheric Environment, 66*, 91–100.

Pasteris, G., Werner, D., Kaufmann, K., & Hohener, P. (2002). Vapor phase transport and biodegradation of volatile fuel compounds in the unsaturated zone: A large scale lysimeter experiment. *Environmental Science & Technology, 36*, 30–39.

Pihlatie, M. K., Christiansen, J. R., Aaltonen, H., Korhonen, J. F. J., Nordbo, A., Rasilo, T., Benanti, G., Giebels, M., Helmy, M., Sheehy, J., Jones, S., Juszczak, R., Klefoth, R., Lobo-do-Vale, R., Rosa, A. P., Schreiber, P., Serça, D., Vicca, S., Wolf, B., & Pumpanen, J. (2013). Comparison of static chambers to measure $CH_4$ emissions from soils. *Agricultural and Forest Meteorology, 171–172*, 124–136.

Pumpanen, J., Kolari, P., Ilvesniemi, H., Minkkinen, K., Vesala, T., Niinisto, S., Lohila, A., Larmola, T., Morero, M., Pihlatie, M., Janssens, I., Yuste, J. C., Grunzweig, J. M., Reth, S., Subke, J. A., Savage, K., Kutsch, W., Ostreng, G., Ziegler, W., Anthoni, P., Lindroth, A., & Hari, P. (2004). Comparison of different chamber techniques for measuring soil $CO_2$ efflux. *Agricultural and Forest Meteorology, 123*, 159–176.

Reid, C. R., Prausnitz, J. M., & Sherwood, T. K. (1977). *The properties of gases and liquids* (3rd ed.). New York: McGraw-Hill.

Rochette, P. (2011). Towards a standard non-steady-state chamber methodology for measuring soil $N_2O$ emissions. *Animal Feed Science and Technology, 166–167*, 141–146.

Rusyn, I., Chiu, W. A., Lash, L. H., Kromhout, H., Hansen, J., & Guyton, K. Z. (2014). Trichloroethylene: mechanistic, epidemiologic and other supporting evidence of carcinogenic hazard. *Pharmacology & Therapeutics, 141*, 55–68.

Sihota, N. J., Mayer, K. U., Toso, M. A., & Atwater, J. F. (2013). Methane emissions and contaminant degradation rates at sites affected by accidental releases of denatured fuel-grade ethanol. *Journal of Contaminant Hydrology, 151*, 1–15.

Sleep, B. E., & Sykes, J. F. (1989). Modeling the transport of volatile organics in variably saturated media. *Water Resources Research, 25*, 81–92.

Smith, J. A., Tisdale, A. K., & Cho, H. J. (1996). Quantification of Natural Vapor Fluxes of Trichloroethene in the unsaturated zone at Picatinny Arsenal, New Jersey. *Environmental Science & Technology, 30*, 2243–2250.

Thomson, N. R., Sykes, J. F., & Vliet, D. V. (1997). A numerical investigation into factors affecting gas and aqueous phase plumes in the subsurface. *Journal of Contaminant Hydrology, 28*, 39–70.

Tillman, F.D. (2003). *Design and testing of a chamber device to measure total flux of volatile organic compounds from the unsaturated zone under natural conditions*, Ph.D. dissertation, University of Virginia.

Tillman, F. D., Choi, J. W., & Smith, J. A. (2003). A comparison of direct measurement and model simulation of total flux of volatile organic compounds from the subsurface to the atmosphere under natural field conditions. *Water Resources Research, 39*, 1284–1295.

Traverse, S., Schäfer, G., Chastanet, J., Hulot, C., Perronnet, K., Collignan, B., Cotel, S., Marcoux, M., Côme, J.M., Correa, J., Gay, G., Quintard, M., & Pepin, L. (2013). Projet FLUXOBAT. *Evaluation des transferts de COV du sol vers l'air int rieur et ext rieur*. Guide m thodologique.

Tuli, A., Hopmans, J. W., Rolston, D. E., & Moldrup, P. (2005). Comparison of air and water permeability between disturbed and undisturbed soils. *Soil Science Society of America Journal, 69*, 1361–1371.

Wallschlager, D., Turner, R. R., London, J., Ebinghaus, R., Kock, H. H., Sommar, J., & Xiao, Z. (1999). Factors affecting the measurement of mercury emissions from soils with flux chambers. *Journal of Geophysical Research, 104*, 21859–21871.

Wang, J. M., Murphy, J. G., Geddes, J. A., Winsborough, C. L., Basiliko, N., & Thomas, S. C. (2013). Methane fluxes measured by eddy covariance and static chamber techniques at a temperate forest in central Ontario, Canada. *Biogeosciences, 10*, 4371–4382.

Yu, L., Wang, H., Wang, G., Song, W., Huang, Y., Li, S. G., Liang, N., Tang, Y., & He, J. S. (2013). A comparison of methane emission measurements using eddy covariance and manual and automated chamber-based techniques in Tibetan Plateau alpine wetland. *Environmental Pollution, 181*, 81–90.